Available online at www.sciencedirect.com
ScienceDirect
Polymer 48 (2007) 2444–2452
polymer
www.elsevier.com/locate/polymer

Stretching of self-interacting wormlike macromolecules

Peter Cifra, Tomáš Bleha*

Polymer Institute, Slovak Academy of Sciences, Dubravska cesta 9, 842 36 Bratislava, Slovakia

Received 30 October 2006; received in revised form 9 February 2007; accepted 12 February 2007
Available online 16 February 2007

Abstract

Structural and elastic properties of non-charged polymers of stiffness ranging from flexible to rigid chains are computed by Monte Carlo simulations. A discrete wormlike chain (WLC) model with self-interacting units is applied to chains of intermediate lengths of interest in the AFM measurements. Variations of the persistence length and mean chain dimensions with bending stiffness are presented. The chain-end distribution functions, the Helmholtz elastic energy and the force–extension profiles of chains of variable stiffness are computed in an isometric ensemble. Occurrence of a plateau on the force–extension curves at intermediate chain stiffness is noted. Qualitative differences are found between force profiles from simulations and from the standard (ideal) WLC model. The differences can be ascribed to an inherent dissimilarity between isometric and isotensional ensembles used and, at small extensions, to the excluded-volume effects. The single-chain functions from simulations were employed to investigate the influence of bending stiffness on elasticity of networks of semiflexible chains by the three-chain model. A stark reduction of degree of elongation of a network with rising stiffness is found. Stress–strain relations show a highly non-linear behavior with the marked strain-stiffening effect.

Keywords: Wormlike chain model; Monte Carlo simulations; Three-chain network model

1. Introduction

Recent experimental investigations of the elastic properties of single biological molecules led to renewal of interest in accurate models of semiflexible macromolecules. A semiflexible chain, which has a conformation intermediate between a random coil and a straight rod may be visualized as a bending wire. A good theoretical understanding of semiflexible polymers is essential in order to correctly interpret the single-molecule experiments studied by the AFM and related techniques [1,2]. These methods offer powerful and versatile tools to measure the force–extension curves in single macromolecules in various situations. Most of such works to date have been conducted on complex biological polymers, such as DNA, proteins, titin and actin, where the data on the response of molecules to external force give new insights into basic biological processes. Single-chain stretching data on synthetic polymers are of profound importance in answering open problems in polymer material science.

Currently the AFM force–length profiles are almost exclusively interpreted by using the two statistical mechanics models of ideal chains, the freely jointed chain (FJC) and the wormlike chain (WLC) models [3–6]. In the FJC model a polymer is described as a chain of randomly jointed N segments of equal (Kuhn) length l_K with no interaction between the segments. Stretching is accompanied solely by the reduction of the conformational entropy of the chain. The WLC model, appropriate for ideal stiff polymers, avoids the segmental approach and a chain describes as a string of constant bending elasticity. The WLC model ignores self-avoidance and its energy is given just by the energy due to curvature. A quantitative measure of the chain stiffness in WLC model is the persistence length l_p, the characteristic length of tangent–tangent orientation correlations of bonds along the chain. Both models neglect the subtle features of chain elasticity ensuing from the specific atomic structure of a molecule. In

* Corresponding author. Fax: +421 2 5477 5923.
E-mail address: bleha@savba.sk (T. Bleha).

0032-3861/$ - see front matter © 2007 Elsevier Ltd. All rights reserved.
doi:10.1016/j.polymer.2007.02.031

fitting the AFM force–length profiles the parameters of the models are treated as the freely adjustable quantities. Thus the WLC fitting constants may considerably differ from the real values of parameters obtained by the polymer solution methods.

In thermodynamic analysis of stretching experiments and calculations two distinct situations have to be considered [3,7–11]: one considers a polymer whose ends are kept at fixed end-to-end distance and measures (by a sensor) the fluctuating force. The result is a plot of mean force as a function of an independent variable, $\langle f \rangle$ *vs* R. In statistical mechanics this condition corresponds to the isometric ensemble (R-ensemble). Alternatively, one can apply a fixed force f and measure the fluctuating end-to-end distance; the result is a plot of $\langle R \rangle$ *vs* f, i.e. of the mean length as a function of an independent variable f. Such a set-up corresponds to the isotensional ensemble (f-ensemble). These conjugated single-chain ensembles can be seen as polymer counterparts of isochoric and isobaric systems, characterized by the Helmholtz and Gibbs energies A and G, respectively. For macroscopic systems two ensembles are related by the usual Legendre transform $G = A - fR$. However, on the single-molecule level, due to large fluctuations in the measured lengths or forces, a choice of statistical ensemble has a profound influence on measured or computed elastic response [3,7–11].

Isotensional conditions were considered in derivations of the force–extension relations for ideal chains. The dependence of the mean chain length $\langle R \rangle$ on the applied force f in the FJC model is expressed by the Langevin function [4] accounting for the limited extensibility of a chain up to a maximum at the contour length L_c. Similarly in the WLC model the force–extension relation was originally deduced for isotensional conditions [5,6]. The resulting approximate interpolation formula [6] became popular in fitting the AFM results of stiff chains such as double-stranded DNA.

A central quantity characterizing elasticity of single macromolecules at isometric conditions is the distribution function of the end-to-end distance $W(R)$. Such distribution functions, the related thermodynamic functions and force – extension curves are available from analytical calculations and computer simulations for a variety of chain models. The FJC model at low extensions reduces to the classical Gaussian model of random-coil elasticity, where the end-to-end distribution function $W(R)$ is given by the Gaussian function [3,4]. In the WLC model a formula for $W(R)$ was deduced initially for rather rigid polymers where the ratio L_c/l_p is of order of one [12]. A general solution of the function $W(R)$ in the WLC model became available only recently from an analytical theory [13] and computer simulations [14]. Lately, the distribution functions and the isometric and isotensional force–extension relations were calculated [15] for a special analytical model of an ideal semiflexible chain. This model assumes a molecule with the Gaussian distribution of distances between successive points along the chain, that is, with the fluctuating value of the contour length L_c.

Elastic properties of non-ideal (self-interacting) chains have been investigated mainly in flexible macromolecules under isometric conditions. Computer modeling by the RIS model or Monte Carlo (MC) and molecular dynamics simulations using a variety of models from coarse-grained to atomistic ones invariably predicts the non-linear force–extension curves [16–23]. The non-Gaussian effects found in the distribution function $W(R)$ and force–extension relations are markedly influenced by the solvent quality [16,17]. Both energy and entropy factors contribute to the force and their proportion can be deduced from the thermoelastic properties of single chains [19–22]. From the single-chain elastic functions stress–strain isotherms were computed for a large variety of elastomeric networks by using the three-chain model of rubber-like elasticity [4,23,24].

In simulations of elastic properties of semiflexible macromolecules a discrete version of the continuous WLC model is usually employed. An inclusion of monomer–monomer self-interaction [25,26] into such a bead-spring chain model mimics the excluded-volume (EV) effect and variable solvent conditions. It was argued [6] that the self-avoidance effects are unimportant for charged macromolecules such as DNA at intermediate and high extension. However, a range of non-charged polymers, including aromatic amides and similar heat-resistant and high modulus polymers, various thermotropic liquid crystalline polymers and numerous polysaccharides, belong to semiflexible polymers. Since good solvents are mostly used in experiments with these polymers, stiff chains may exhibit deviations from ideal chain behavior due to EV interactions, particularly in the limit of very long chains [27]. On the other hand, polymers of intermediate length are of primary experimental interest in the AFM method. Here as well an impact of the EV effect on the force–extension profiles calls for closer examination.

In the present paper we have simulated the behavior of non-charged polymers of stiffness ranging from flexible to almost rigid chains by means of the discrete WLC-like model involving self-interacting segments. At first, variation of the persistence length with bending stiffness was calculated and the role of EV was elucidated. Then, the chain-end distribution functions, the Helmholtz elastic energy and force–extension curves were computed under isometric boundary conditions. Finally, influence of bending stiffness on elasticity of networks of semiflexible chains was investigated by the three-chain model of rubber-like elasticity.

2. Simulation model

We have used a hybrid coarse-grained model of semiflexible chains in which the FJC-like segmental approach is combined with the WLC-like bending energy. A chain in the model consists of bead units connected by effective bonds characterized by stiff springs. Each effective bond represents several chemical bonds along the chain backbone. Additionally, a potential for self-interaction of effective units is included in this discretized analogy of the WLC model. An effective bond is described by finitely extensible non-linear elastic potential (FENE) [28]

$$U_{\mathrm{FENE}}(l) = -\kappa r^2 \ln\left[1 - \left(\frac{l - l_o}{r}\right)^2\right] \quad (1)$$

The bond length in the potential varies between $l_{\min} = 2l_o - l_{\max}$ and $l_{\max}$, where l_o is a preferred distance, $r = l_{\max} - l_o$, the bond stretching constant $\kappa = 20\varepsilon$ and ε is the strength of pair-contact interaction. Typical distances are $l_{\min} = 0.4$, $l_o = 0.7$ and $l_{\max} = 1$. The FENE potential introduces the fluctuating contour length into the model, in analogy with an approach [15] modeling the WLC polymer with a Gaussian distribution of distances between successive points along the chain. Yet, the minimum changes of L_c were found in simulations.

Variation in chain stiffness is expressed by the bending potential [29,30] between two consecutive bonds,

$$U_b = b(1 - \cos\theta) \quad (2)$$

where θ is a supplementary angle to a valence angle and the stiffness parameter (the bending force constant) $b = A\varepsilon$ is proportional to the pair-contact interaction energy.

A Morse-type potential [28] is used for the non-bonded interactions between effective monomeric units (beads) separated by distance r. Incorporation of non-bonded interaction of monomers introduces the EV effect into the model. The potential includes a quasi-hard core self-avoidance and an attraction part

$$U_M(r)/\varepsilon = \exp[-2\alpha(r - r_{\min})] - 2\exp[-\alpha(r - r_{\min})] \quad (3)$$

where $\alpha = 24$ and the minimum of the potential $r_{\min} = 0.8$ was selected [28]. This short-range potential predicts negligible interaction at $r \geq 1$ and the closest distance of monomer units at ≈ 0.76. Thus, the core radius of a bead is $\sigma \approx 0.38$. All distances in the above potentials are expressed in arbitrary length units.

A similar model was recently used to examine the behavior of grafted WLC polymers under mechanical stress [26]. The principle parameters of the model are the chain stiffness b (related to the persistence length l_p) and the pair interaction energy ε. The parameters representing the good solvent condition were selected in the potentials, Eqs. (1)–(3). By turning interaction potential $U_M(r)$ on and off it is possible to assess the contribution of EV interactions to computed properties of chains. When the temperature is expressed in units of the Boltzmann constant and the unit strength of the attractive potential, $\varepsilon/k = 1$, is chosen, simulations correspond to the temperature $T = 1$, well above the theta state located at temperature about $\Theta \approx 0.62$ [28].

Metropolis MC method with reptation updates of chains was used to obtain the ensemble averages. No biasing technique for sampling semiflexible chains was used. The trial moves were created completely randomly and accepted with classical Metropolis criterion. Thus acceptance of very stiff chains was relatively low (only few percent for highest stiffness). Number of trial moves used in chain generation was up to 3×10^7 MC cycles. The validity of algorithm was checked by reproducing some of the universal coil properties. For flexible chains we found the size ratio $\langle R^2\rangle/\langle R_g^2\rangle = 6.34$ close to theoretical value 6.303 and for semiflexible chains we observed locally (in high q-limit) the coil form factor $S(q) \sim q^{-1}$ characteristic for rigid rod. Error estimates of ensemble averages are for most depicted results within the size of markers except for end-to-end distance distributions in region of $R \to 0$ where slightly larger fluctuations can be explained by poorer sampling of quasi-cyclic conformations. Single chains of lengths N from 20 to 400 units were generated. Mostly the results for the chain length of 100 and 200 beads are given, representing the polymers of intermediate lengths typical in AFM measurements. The stiffness parameter b was varied in the interval 0–75. The radial distribution function of end-to-end distances $P(R)$ was evaluated by grouping the chain vector lengths from the simulations into a histogram of a bin width of 0.7. Furthermore, the mean-square end-to-end distance $\langle R^2\rangle$, the radius of gyration $\langle R_g^2\rangle^{1/2}$ and two WLC parameters, the contour length, $L_c = (N-1)\langle l\rangle$ and the persistence length l_p were computed from simulations. The persistence length l_p was calculated by two methods [3,31]: (a) by the rigorous definition, from the average sum of projections of all bonds on the first bond of a chain in the limit $N \to \infty$

$$l_p = \left\langle \sum_{i=1}^{N-1} \vec{l}_i \vec{l}_1 \right\rangle \Big/ \langle l\rangle \quad (4)$$

and (b) by the approximate procedure from the average cosine of the supplementary angle in the chain backbone

$$l_p = \langle l\rangle/(1 - \langle\cos\theta\rangle) \quad (5)$$

The latter equation applies for a wormlike chain and is deduced as a continuous limit of a freely rotating chain by letting $N \to \infty$, $\Theta \to 0$ and $l \to 0$ [27].

3. Results and discussion

3.1. Chain structure parameters

At first, the dependence of the persistence length l_p defined by Eq. (4) on the chain length N was computed for self-interacting chains (Fig. 1). All values of l_p and of other length quantities presented in figures henceforth are normalized by the unit bond length $l_o = 0.7$. In the range of chain stiffness considered the chain length $N = 400$ is apparently sufficient to reach the limiting value $(l_p)_\infty$ at $N \to \infty$. The set of extrapolated values of $(l_p)_\infty$ for self-interacting chains, denoted henceforth as the rigorous persistence lengths, is plotted in Fig. 2 as a function of the stiffness parameter b. The persistence length $(l_p)_\infty$ increases linearly with the parameter b and the resulting straight line in Fig. 2 gives the slope very close to unity. The plot in Fig. 2 upholds a direct proportionality between the bending force constant b and persistence length $(l_p)_\infty$ for a continuous chain [29]

$$b = kT(l_p)_\infty/l_o$$

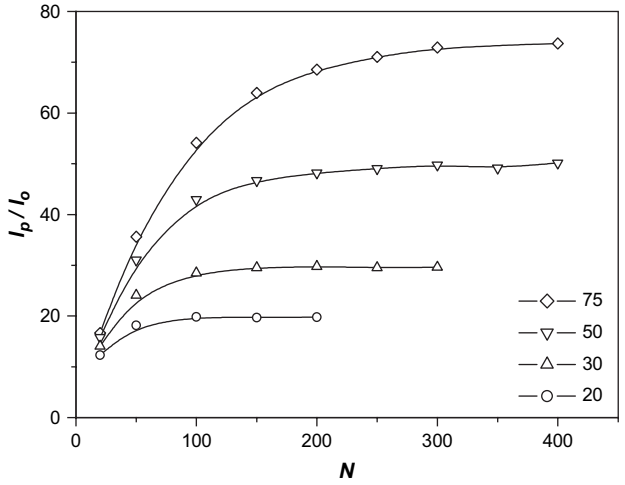

Fig. 1. Variation of the persistence length l_p based on Eq. (4) with the chain length N for the stiffness parameter b given in the legend.

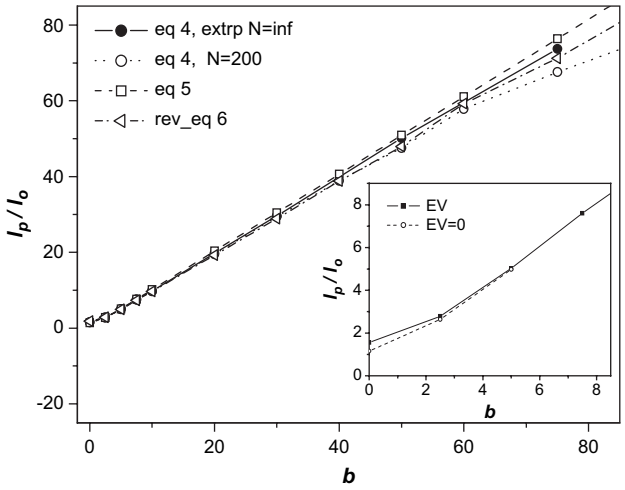

Fig. 2. Variation of the persistence length with the stiffness parameter b computed for self-interacting (EV) chains by Eq. (4) from the extrapolated values $(l_p)_\infty$ (solid circles) and from the values of l_p for $N = 200$ (empty circles); by Eq. (5) (squares) and by the reverse manner from WLC mean dimensions given by Eq. (6) (triangles). Inset: persistence length from Eq. (4) for non-interacting chains (EV = 0) computed by setting $U_M = 0$ (dotted line).

calculated analytically from the description of chain stiffness in terms of elasticity theory and taking into account that reduced units $kT = 1$ are implied in simulations.

Exploitation of values of the persistence length based on Eq. (4) without extrapolation to $N \to \infty$ is as a rule inappropriate. The use of unextrapolated values, such as $(l_p)_{200}$ corresponding to $N = 200$, leads to a deviation from linearity in Fig. 2 at higher chain stiffness. Furthermore, the persistence length computed from the average cosine by Eq. (5) is plotted in Fig. 2. As seen, in the range of chain stiffness considered this approximate procedure gives about the same values of l_p for a given b as the rigorous procedure.

The dependences of l_p on b for pseudo-ideal chains, modeled by neglecting non-bonded interaction and denoted EV = 0, are almost identical to those for self-interacting chains; some minute difference can only be seen in the low stiffness region (inset of Fig. 2). Hence, the volume effects influence persistence length only in fairly flexible chains; for b higher than about 5 the persistence length is essentially identical to the "unperturbed" value $(l_p)_\Theta$ pertaining to the theta state.

Variation of the mean-square end-to-end distance $\langle R^2 \rangle$ with the stiffness parameter b is shown in Fig. 3. Mean dimensions increase monotonously with chain stiffness. At small b a random-coil regime is present, as documented by the ratio $\langle R^2 \rangle / \langle R_g^2 \rangle = 6.34$ for $b = 0$ and $N = 200$, typical for flexible chains in good solvents. Mean chain dimensions gradually increase as the chains become stiffer, but even at $b = 75$ the ratio $\langle R^2 \rangle / \langle R_g^2 \rangle = 9.10$ for $N = 200$ is still off the rigid-rod limit of 12. The EV effect on dimensions $\langle R^2 \rangle$ is hardly noticeable in Fig. 3 and, again, is limited only to flexible chains.

Predictions of the chain size by the standard (ideal) WLC model are also plotted in Fig. 3. The mean-square end-to-end distance of WLC is given as [3,27]

$$\langle R^2 \rangle_{\mathrm{WLC}} = 2 l_p L_c - 2 l_p^2 \left(1 - \exp\left(-L_c / l_p\right)\right) \tag{6}$$

The function $\langle R^2 \rangle_{\mathrm{WLC}}$ was computed by using the contour length $L_c = 199 \langle l \rangle$ and extrapolated values of $(l_p)_\infty$ for self-interacting chains. As seen in Fig. 3 chain dimensions from the standard WLC model are in harmony with the simulation results.

A variety of experimental methods are used to determine l_p in dilute solutions or in bulk, including viscosity, sedimentation, flow birefringence, light scattering and SANS [27]. The experimental data (obtained mostly in good solvents) are fitted with the standard (ideal) WLC model and the potential EV effect on the persistence length is neglected. In other words, Eq. (6) (or its pendant for the radius of gyration [27]) is used in reverse to determine the persistence length from the measured chain dimensions. In order to illustrate this procedure, the simulation data of $\langle R^2 \rangle$ were substituted into

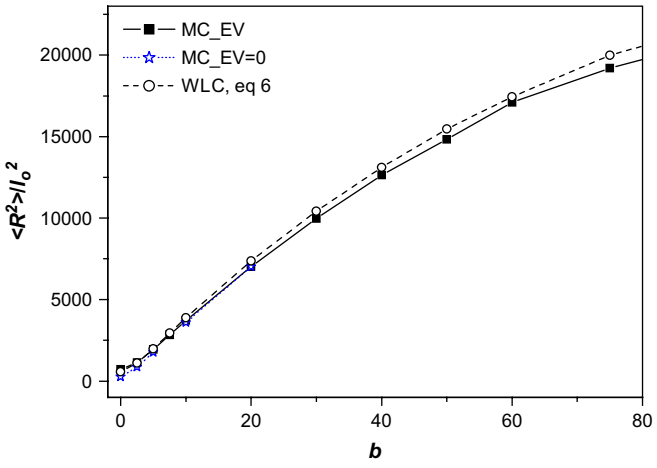

Fig. 3. Variation of the chain dimensions $\langle R^2 \rangle$ with chain stiffness b for $N = 200$ determined by MC simulations with EV interactions included or neglected (squares and stars, respectively) and computed from the WLC relation, Eq. (6), by using extrapolated values of $(l_p)_\infty$ for self-interacting chains (dashed line).

Eq. (6) and the values of l_p extracted. The persistence length computed in such a reverse manner from WLC mean dimensions (Fig. 2) fully concurs with the corresponding values based on Eqs. (4) and (5). It was noted earlier [31] that various definitional expressions for computing the persistence length in semiflexible chains may result in disparate values of persistence length for very rigid chains if persistence length is not extrapolated to $N \to \infty$.

Instead of the model-based stiffness parameter b, the ratio of the contour and persistence lengths L_c/l_p can be employed as an alternate indicator of the chain stiffness. This ratio of two experimentally accessible quantities is in a reciprocal relation to the parameter b. The function L_c/l_p *vs* b calculated by using the rigorous persistence lengths is illustrated in Fig. 4 for four chain lengths. Conventionally, a chain is considered flexible when $L_c \gg l_p$ and rigid when $L_c \approx l_p$ holds. The respective limits $L_c/l_p \to \infty$ and $L_c/l_p \to 0$ represent a Gaussian random coil and a rigid rod. The semiflexible chains cover a wide range of parameters L_c/l_p or b between the above limits.

3.2. Chain-end distributions and the Helmholtz energy

When the chain length R is taken as independent variable the elastic response of a single macromolecule is derived from the co-ordinate probability distribution function $W(R)$ of a macromolecule having one end fixed at the origin and the other end fixed in space at co-ordinates x,y,z. The distribution function $W(R)$ of a chain of contour length L_c is related [3,4] to the Helmholtz elastic energy $A = c(T) - kT \ln W(R)$. Since the mean configurational Helmholtz energy of an unconstrained chain $c(T)$ is a function only of T it will be henceforth incorporated into A. The probability distribution functions $W(R)$ is linked to the radial function of a chain with a free end point by $W(R) = P(R)/4\pi R^2$.

The change of the radial distribution functions $P(R)$ on going from flexible to almost rigid chains is shown in Fig. 5a. Error bars in simulation data are approximately of the size of symbols. On increasing chain stiffness the peak maximum shifts to the larger chain-end distances R. In flexible chains the $P(R)$ distribution is controlled primarily by the conformational entropy whereas the bending potential that tries to extend the chain prevails in semiflexible chains. These competing trends affect also the changes of the distribution function $W(R)$ with the chain stiffness b (not shown): while the flexible chains can roughly be described by the Gaussian function, the distribution function $W(R)$ takes a completely non-Gaussian shape in the region of semiflexible chains. On the distribution $P(R)$ it is seen once more that EV interactions play a role only in flexible chains of $b < 5$ (Fig. 5b).

The Helmholtz elastic energy $A(R)$ of chains of variable stiffness expressed by the parameter b is presented in Fig. 6a. The trends in distribution functions and Helmholtz energy observed for self-interacting chain model are qualitatively similar to the findings reported for the standard [12–14] and Winkler [15] WLC models. A roughly Gaussian quadratic dependence of A on R is seen in Fig. 6a in flexible

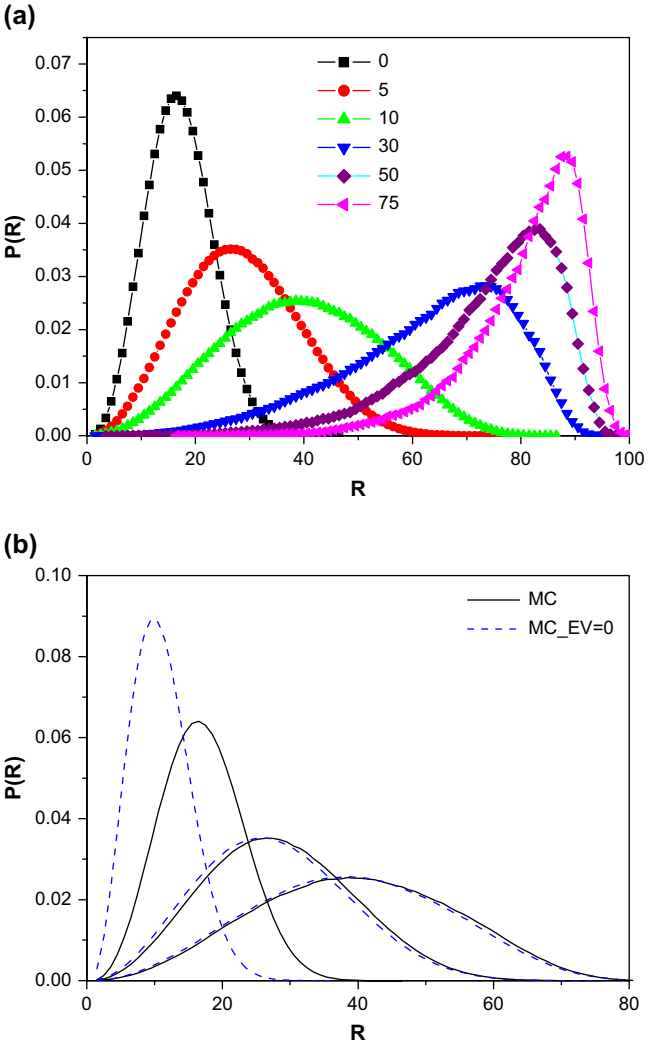

Fig. 5. (a) Radial distribution functions of chains of $N = 100$ and stiffness b given in the legend and (b) the corresponding functions for $b = 0$, 5 and 10 (from left to right) computed by simulations with (full lines) and without (dashed lines) non-bonded interactions.

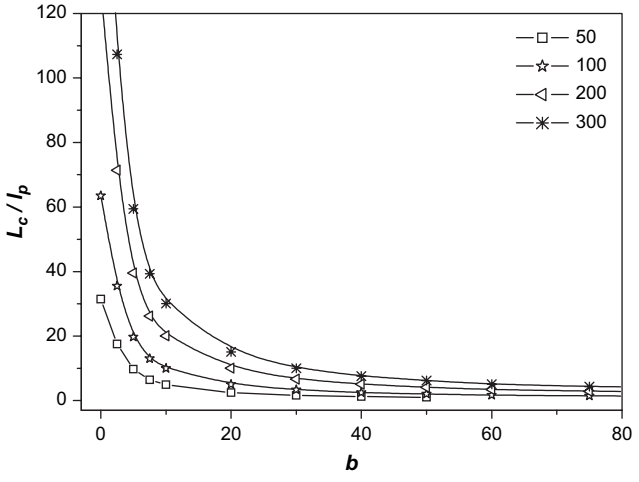

Fig. 4. The dependence of ratio of the contour and persistence lengths L_c/l_p on the stiffness parameter b for chain lengths N given in the legend.

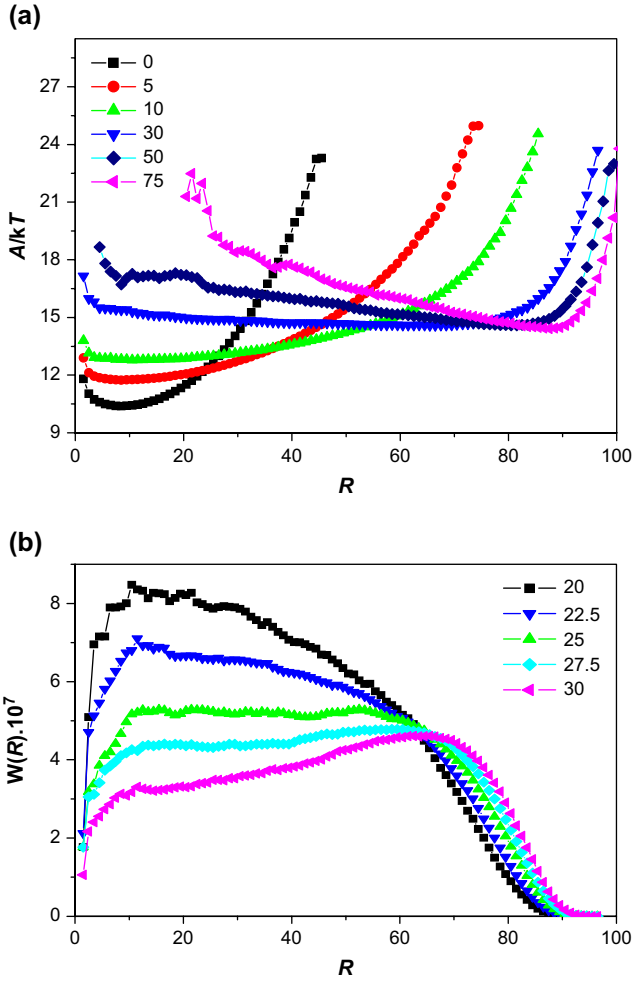

Fig. 6. (a) Helmholtz elastic energy and (b) probability distribution function $W(R)$ in the crossover region for chains of $N = 100$ and the bending parameter b given in the legend.

chains, except at $R \to 0$ where, in contrast to ideal chains, a ring closure probability is zero due to the EV effect. The minima on the Helmholtz energy curves move towards full chain stretching with increasing chain stiffness and a positive inclination of $A(R)$ curves in the central region changes to a negative one.

The behavior in a crossover region between flexible and rigid chains is particularly intriguing as illustrated by the shape of the function $W(R)$ shown in Fig. 6b. A long, roughly flat section of the function $W(R)$ is observed at intermediate stiffness around $b = 25$ ($L_c/l_p = 4.06$ for $N = 100$). A non-monotonic behavior of $W(R)$ and $A(R)$ functions with double minimum hump was discovered in the standard WLC model [13,14] for a range of persistence lengths near to $L_c/l_p = 3.85$. Such a behavior invokes the first-order transition where a chain could co-exist in a "short" (flexible) and a "long" (rigid rod) state and leads to curious force–length relation. Bimodality of this type was not found by Winkler in his WLC model [15] and is not seen in Fig. 6b for our discrete WLC-like model at intermediate chain lengths. The contour length fluctuations assumed in our and Winkler models may be responsible for this notable dissimilarity in behavior relative to the standard WLC model.

3.3. Force–extension functions

The mean force as a function of an independent variable R is determined by the differentiation $\langle f \rangle = \mathrm{d}A/\mathrm{d}R$. The forces and extensions are taken to be along the z axis. The curves $\langle f \rangle(R)$ markedly change along the transition from flexible to stiff chains and the highly non-linear force–length functions are observed (Fig. 7). A quasi-linear region of entropy elasticity is followed on curves by an upturn to higher forces. This upturn occurs at high chain extensions in stiff chains and becomes very steep. In flexible chains the compression forces $\langle f \rangle < 0$ are present only at small R. However, in stiff chains the compressive force is predicted almost through all chain extensions. In harmony with the shape of Helmholtz elastic energy $A(R)$ only one zero-force point (at finite extension) is present on each curve $\langle f \rangle(R)$ in Fig. 7. In absence of the EV effect an additional zero-force point would be seen at zero extension [15]. Again, the zone of intermediate chain stiffness is worthy of note. In less stiff chains with b below 25 ($L_c/l_p = 4.06$ for $N = 100$), a plateau is found in wide region of R featuring small positive mean force. Above this crossover value of b such a plateau corresponds to small negative (compressive) forces. Around the square-root of end-to-end distance $\langle R^2 \rangle^{1/2}$ a force plateau changes to a force upturn. A potentially non-monotonic shape of the force–extension curve in the crossover region would display a van der Waals' loop and a region of instability [17].

Force–extension curves of semiflexible chains obtained by the AFM methods are commonly interpreted [1,2] by the WLC model using the approximate relation [6] derived from isotensional considerations

$$\frac{f l_p}{kT} = \frac{1}{4(1-x)^2} - \frac{1}{4} + x \tag{7}$$

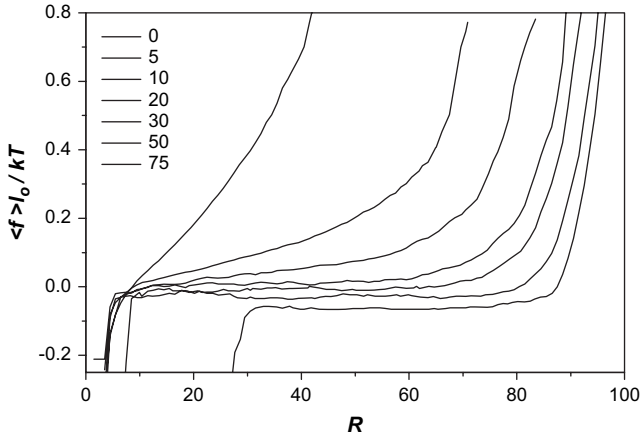

Fig. 7. The mean force $\langle f \rangle$ as a function of chain elongation R calculated for semiflexible chains at isometric conditions for chains of $N = 100$ and the bending parameter b in the legend in the order of lines from left to right.

where $x = \langle R_z \rangle / L_c$ and $\langle R_z \rangle$ is the mean elongation along the direction of the force. The formula accurately represents the small and large force regimes but has a maximum error of 10% in the intermediate force regime [6]. We have computed the force–extension profiles $\langle R_z \rangle$ *vs* f by substituting the persistence lengths calculated by Eqs. (4) and (5) into the WLC interpolation formula. The results for chain length $N = 100$ are compared in Fig. 8 with curves $\langle f \rangle$ *vs* R from our isometric simulations.

Significant differences are seen in Fig. 8 between elastic response from simulations and from WLC interpolation formula. First of all, the WLC profiles are shifted to lower extension in comparison with the corresponding isometric profiles from simulations. Then, only positive forces, all starting from origin, are present in the isotensional WLC profiles. Region of long plateau of nearly zero forces found in simulations in the crossover region at intermediate chain stiffness is absent in the WLC profiles. These differences become especially striking in stiff chains where simulations predict compressive forces up to very high chain extensions. This assessment validates the notion that the persistence lengths obtained from fitting the experimental force–extension profiles (at a given contour length) correspond to apparent parameters and not to the real chain characteristics.

Several factors contribute in Fig. 8 to disparity of curves from our discretized self-interacting WLC model and the standard WLC model, including contour length fluctuations, EV interactions, and boundary conditions used. Although, in contrast to the standard WLC model, fluctuations in contour length of simulated chains were allowed, in reality the minimum changes of L_c were observed in simulations. The EV effects in simulation curves in Fig. 8 are confined only to low extensions R/L_c. Major influence on elastic functions arises from a choice of a statistical ensemble. Because of fluctuations in the measured lengths or forces on the single-molecule level,

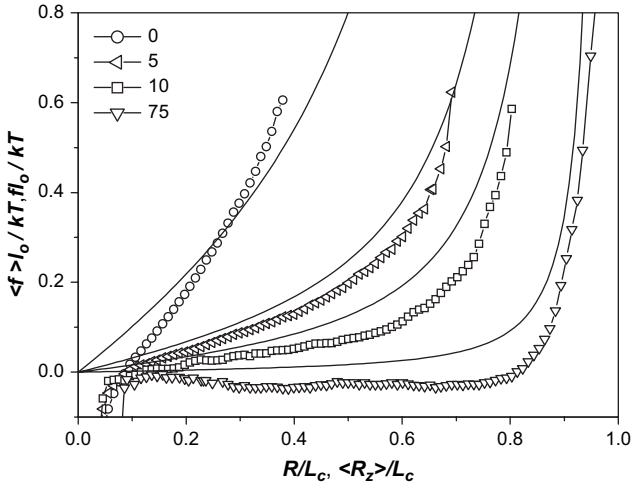

Fig. 8. Pairs of force–extension curves of semiflexible chains for chains of $N = 100$ and the bending parameter b given in the legend computed from simulations at isometric conditions (symbols) and from the WLC interpolation formula (Eq. (7)) by using the extrapolated persistence lengths $(l_p)_\infty$ (full lines).

the Helmholtz and Gibbs elastic energies are not related by the Legendre transform. The $\langle f \rangle(R)$ relations are different from the $\langle R_z \rangle(f)$ relations even in a case of the structurally simplest polymer, polyethylene [10,19]. Only if fluctuations about the averages are ignored the designation of averages can be abandoned and f and R variables can be transposed. In the limit of infinite flexibility $L_c/l_p \to \infty$ two ensembles would give the same force–extension curves in non-interacting chains whereas the dissimilarities would be preserved in case of self-interacting chains.

3.4. Three-chain model of networks

The single-chain Helmholtz elastic energy and the functional dependence of the mean force $\langle f \rangle$ on R form a foundation of time-honoured theories of network elasticity. Models based on the behavior of set of "average" chains are conventionally used in computations of elastic properties of polymer networks [4,23,24,32–34]. The bending stiffness of chains introduces a new microscopic parameter that has a consequence for the traditional rubber-elasticity model of networks formed by crosslinked flexible polymers. It is frequently assumed that stiffening of network is ensuing primarily from longitudinal stiffening of polymer strands themselves. A contour length relevant in networks is the distance between network junction points (crosslinks).

For the isometric single-chain functions presented in Figs. 6 and 7 we have employed the three-chain model of a network. This approach, mostly exploited for flexible chains [4,16,17,23,24] ought to be suitable also for not too stiff polymers. The model assumes that the Helmholtz elastic energies of chains are averaged in three orthogonal orientations. The effective chains with the end-to-end distances R_i $(i = x,y,z)$ parallel to the co-ordinate axes are deformed in the affine limit at constant volume, i.e. the crosslinks move linearly with the macroscopic dimensions of the sample L_i. The respective macroscopic deformations of a sample are defined as elongations $\lambda_i = L_i/L_{i0}$ where subscript zero denotes the undeformed dimensions. In the case of uniaxial elongation ($\lambda_x = \lambda$ and $\lambda_y = \lambda_z = \lambda^{-1/2}$) the Helmholtz energy A_{net} of a model network composed of ν chains per volume unit is given by the difference of the single-chain functions $A(R)$ in the deformed and undeformed states

$$A_{net} = \nu kT\left[A(R_o\lambda_x)/3 + (2/3)A\left(R_o\lambda_y\right) - A(R_o)\right] \tag{8}$$

where $R_o = \langle R^2 \rangle^{1/2}$ are the average chain dimensions of the network chains in the undeformed state.

The Helmholtz energy of a model network A_{net} is plotted in Fig. 9 as a function of elongation λ in wide range of chain stiffness. The Helmholtz energy function in an ideal network of Gaussian chains is given by the relation $A_{G,net}/\nu kT = (1/2)(\lambda^2 + 2\lambda^{-1} - 3)$ which is also shown in Fig. 9. On rising stiffness one can see a stark reduction in degree of elongation λ, a sharp upturn in A_{net} and narrowing of a region around the Helmholtz energy minimum. Interestingly, a similar pattern in variation of A_{net} was observed in simulations of

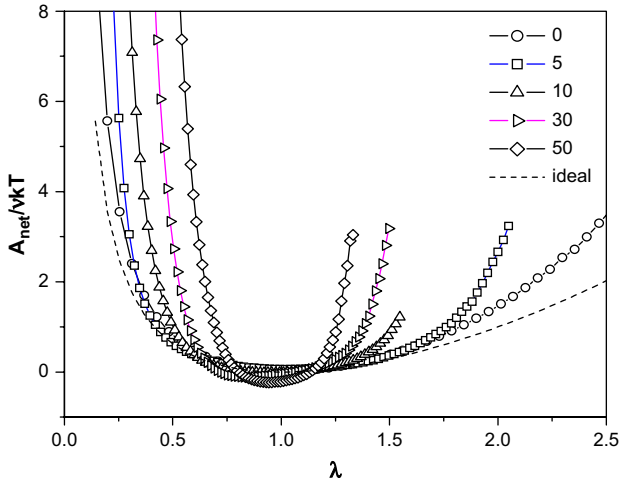

Fig. 9. The Helmholtz energy of the three-chain model of networks computed for the bending parameter b given in the legend. An analogous plot for the ideal network is shown by the dotted line.

model networks of helical polymers as a function of temperature [34].

The differentiation of Eq. (8) with respect to elongation at constant volume and temperature gives the nominal stress σ as a function of isometric single-chain mean forces

$$\sigma = (\nu kTR_o/3)\left[f(R_o\lambda) - \lambda^{-3/2} f\left(R_o\lambda^{-1/2}\right)\right] \tag{9}$$

The two terms in the brackets on the right-hand-side of Eq. (9) account for the extension and lateral compression of the sample, respectively. The stress–strain relations computed for networks of chains of stiffness ranging from fully flexible to rather stiff polymers display in Fig. 10 numerous features of non-linear elasticity. Extensibility of networks is drastically limited by increasing chain stiffness; an analogous compression effect is less pronounced in Fig. 10. The deformation of networks of flexible chains is controlled mainly by entropy,

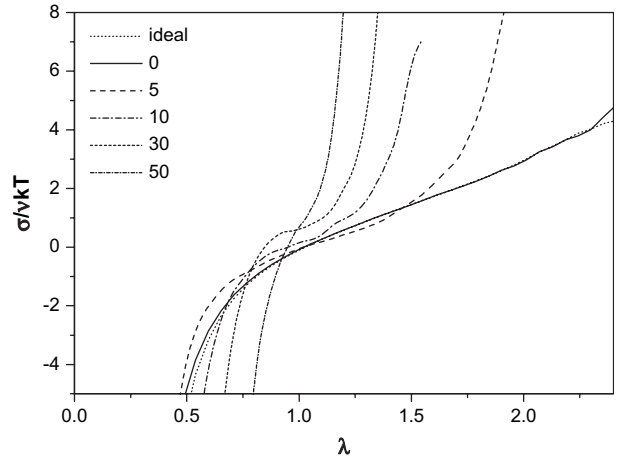

Fig. 10. Stress–strain relations computed for networks of chains with the bending parameter b given in the legend (in the order from right to left in the upper sector). The Gaussian relation for the ideal network (dotted line) almost coincides with line for $b = 0$.

similarly to Gaussian networks. On the other hand, in stiffer chains, the deformation energy is stored primarily in bending of chain segments. Interestingly, a force plateau featured in Fig. 7 on single-chain curves $\langle f\rangle(R)$ in the crossover region of L_c/l_p is no more discernible on stress–strain isotherms of a model network. This hypothetical effect, supposed to occur in networks in a region below and around $\lambda = 1$, is effectively suppressed by the lateral compression term in Eq. (9). Thus, the low-modulus elastic response of single chains is not transformed into equivalent network behavior. The plots in Fig. 10 corroborate the strain-stiffening effect generic for networks composed of semiflexible polymers. The strain at which stiffening becomes significant strongly depends on the persistence length. It is encouraging that stress–strain relations in Fig. 10 qualitatively agree with the results of MC simulations of a much more complex and realistic model of end-linked networks consisting of semiflexible chains [35].

It should be mentioned, however, that the simple model used is suitable just to networks made from not too rigid chains, with little or no entanglements. Numerous inherent limitations of the three-chain model preclude its applicability to stiff networks and entangled networks. For example, nematic mean-field type of interaction may be operative in networks made from semirigid chains resulting in the appearance of an isotropic–nematic transitions at high strains [36]. Furthermore, it is supposed that in flexible polymers the segments between crosslinks behave independently. However, strands in semiflexible networks most likely act in series, since segments of stiff chains remain correlated over much longer distances that is the mesh size of a crosslinked network. Thus the properties of such a network depend both on mesh size and on the contour length of chains [37].

4. Conclusions

A segmental model involving self-avoiding and interacting units, corresponding to a discretized WLC model, was employed in Monte Carlo simulations of chains of stiffness ranging from fully flexible to relatively stiff polymers. The persistence length and mean chain dimensions were calculated for semiflexible polymers of intermediate lengths. Chain stiffness-induced modifications of the chain-end distribution functions, the Helmholtz elastic energy and force–extension curves computed in an isometric ensemble were presented. At intermediate chain stiffness a long plateau on the force–extension curves was observed. Qualitative differences are found between the simulation results and the predictions of the standard WLC model that can be ascribed to excluded-volume effects and to an inherent dissimilarity between isometric and isotensional boundary conditions.

Influence of bending stiffness, a new microscopic parameter in traditional rubber elasticity, was explored by the three-chain model of networks of semiflexible chains. It was found that extensibility of networks is drastically reduced by increasing chain stiffness; an analogous compression effect is less pronounced. The stress–strain isotherms show a highly nonlinear behavior with the marked strain-stiffening effect.

Acknowledgement

This work was supported by Science and Technology Assistance Agency under the contract no. APVT-51-044902 and in part by VEGA, Grant 2/6014/26.

References

[1] Janshoff A, Neitzert M, Oberdörfer Y, Fuchs H. Angew Chem Int Ed 2000;39:3212.
[2] Hugel T, Seitz M. Macromol Rapid Commun 2001;22:989.
[3] Flory PJ. Statistical mechanics of chain molecules. New York: Wiley-Interscience; 1969.
[4] Treloar LRG. The physics of rubber elasticity. Oxford, UK: Clarendon Press; 1975.
[5] Kovac J, Crabb CC. Macromolecules 1982;15:537.
[6] Marko JF, Siggia ED. Macromolecules 1995;28:8759.
[7] Kreuzer HJ, Payne SH, Livadaru L. Biophys J 2001;80:2505.
[8] Keller D, Swigon D, Bustamante C. Biophys J 2003;84:733.
[9] Neumann RM. Biophys J 2003;85:3418.
[10] Zemanová M, Bleha T. Macromol Theory Simul 2005;14:596.
[11] Makarov DE, Wang Z, Thompson JB, Hansma HG. J Chem Phys 2002;116:7760.
[12] Wilhem J, Frey E. Phys Rev Lett 1996;77:2581.
[13] Samuel J, Sinha S. Phys Rev E 2002;66:050801.
[14] Dhar A, Chaudhuri D. Phys Rev Lett 2002;89:065502.
[15] Winkler RG. J Chem Phys 2003;118:2919.
[16] Cifra P, Bleha T. Macromolecules 1998;31:1358.
[17] Cifra P, Bleha T. J Polym Sci Part B Polym Phys 1999;37:2013.
[18] Smith JS, Bedrov D, Smith GD, Kober EM. Macromolecules 2005; 38:8101.
[19] Titantah JT, Pierleoni C, Ryckaert JP. J Chem Phys 2002;117:9028.
[20] Cifra P, Bleha T. J Chem Soc Faraday Trans 1995;91:2465.
[21] Wittkop M, Kreitmeier S, Goritz D. J Chem Soc Faraday Trans 1996;92:1375.
[22] Špitalský Z, Bleha T, Cifra P. Macromol Theory Simul 2002;11:513.
[23] Mark JE, Curro JG. J Chem Phys 1983;79:5705.
[24] Mark JE. J Phys Chem B 2003;107:903.
[25] Rosa A, Hoang TX, Marenduzzo D, Maritan A. Macromolecules 2003;36:10095.
[26] Kneller JM, Elvingston C, Arteca GA. Chem Phys Lett 2005;407:384.
[27] Norisuye T. Prog Polym Sci 1993;18:543.
[28] Milchev A, Binder K. Macromolecules 1996;29:343.
[29] Hakansson C, Elvingson C. Macromolecules 1994;27:3843.
[30] Cifra P. Macromolecules 2005;38:3984.
[31] Cifra P. Polymer 2004;45:5995.
[32] Cail JI, Stepto RFT. Polymer 2003;44:60.
[33] Klockowski A. Polymer 2002;43:1503.
[34] Carri GA, Batman R, Varshney V, Dirama T. Polymer 2005;46:3809.
[35] Bhawe DM, Cohen C, Escobedo FA. Macromolecules 2004;37:3924.
[36] Bahar I, Erman B, Kloczkowski A, Mark JE. Macromolecules 1990; 23:5341.
[37] Head DA, Levine AJ, MacKintosh FC. Phys Rev E 2003;68:061907.